Quantum Chaos Driven by Long-Range Waveguide-Mediated Interactions

Alexander V. Poshakinskiy,[1] Janet Zhong,[2] and Alexander N. Poddubny[1,2,*]
[1]*Ioffe Institute, St. Petersburg 194021, Russia*
[2]*Nonlinear Physics Centre, Research School of Physics, Australian National University, Canberra ACT 2601, Australia*

(Received 27 November 2020; accepted 12 April 2021; published 21 May 2021)

We study theoretically quantum states of a pair of photons interacting with a finite periodic array of two-level atoms in a waveguide. Our calculation reveals two-polariton eigenstates that have a highly irregular wave function in real space. This indicates the Bethe ansatz breakdown and the onset of quantum chaos, in stark contrast to the conventional integrable problem of two interacting bosons in a box. We identify the long-range waveguide-mediated coupling between the atoms as the key ingredient of chaos and nonintegrability. Our results provide new insights in the interplay between order, chaos, and localization in many-body quantum systems and can be tested in state-of-the-art setups of waveguide quantum electrodynamics.

DOI: 10.1103/PhysRevLett.126.203602

Introduction.—Arrays of superconducting qubits or cold atoms coupled to a waveguide have recently become a promising new platform for quantum optics [1–7]. The arrays can be used for storing [8] and generating quantum light [7,9–11] and even for a future "quantum internet" [12]. Moreover, qubit arrays are a new type of quantum simulator for the problems of many-body physics [13–19]. One of the most fundamental problems in physics is the competition between order and chaos, or many-body localization and thermalization. This competition is already a subject of active studies [20,21]: from celestial mechanics to atomic, nuclear [22], and condensed matter [23–25] physics and even to quantum paradoxes in black holes [26,27]. Despite the large diversity of these systems, the consideration is typically limited to excitations with parabolic dispersions and short-range coupling. Arrays of atoms in a waveguide present a unique platform to probe unexplored boundaries of quantum chaos and integrability in a system with strong interactions, long-range waveguide-mediated coupling, and intrinsically nonparabolic dispersion of excitations.

Here, we demonstrate that even a seemingly simple problem of just two photons interacting with a periodic finite array of two-level atoms in a waveguide [Fig. 1(a)] may provide important general insights into quantum chaos. In this setup, the coupling of photons to atoms leads to the formation of polaritons. Polaritons repel each other since a single two-level atom cannot host two resonant photons at the same time [28]. This is strongly reminiscent of an exactly solvable (integrable) one-dimensional model of two bosons in a box that demonstrates fermionization in the limit of strong repulsion [29–31]. The integrability can be broken when the interaction becomes nonlocal [32] or there is an external potential [33] or if the bosons acquire different masses [34], which can be mapped to an irrational-angle billiard [35]. Since the considered polaritons are locally interacting equivalent bosons and there is no external potential, the integrability should persist at the first glance. Indeed, fermionized two-polariton states have been recently revealed by Zhang and Mølmer [36]. However, we later uncovered [37,38] a very different kind of two-polariton state that has a broad Fourier spectrum and

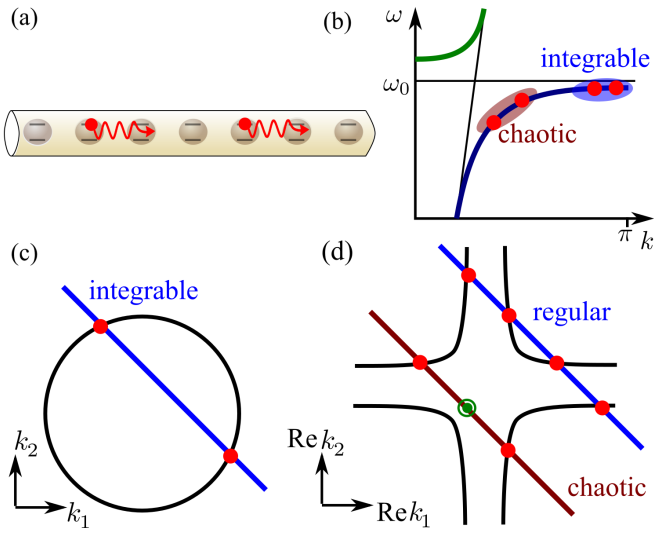

FIG. 1. (a) Schematics of a two-photon state in array of atoms in a waveguide. (b) Schematics of single-polariton dispersion curve $\omega(k)$. Two polaritons pairs with small and large wave vectors corresponding to chaotic and integrable states are indicated. (c),(d) Wave vectors of two-polariton states with the same total energy and momentum for the case of (c) parabolic and (d) nonparabolic $\propto -1/k^2$ single-particle dispersion. Black curves shows the isoenergy contour $\omega(k_1)+\omega(k_2)=\text{const}$. Slanted lines illustrate the total momentum conservation, $k_1+k_2=\text{const}$. Green circle in (d) corresponds to the complex $k_{1,2}$, with real part lying outside the isoenergy contour.

cannot be reduced to a product of several single-particle states. This hints that the problem is nonintegrable by the Bethe ansatz, but the mechanism and consequences of nonintegrability remain unclear.

In this Letter, we find chaotic two-polariton eigenstates that differ from previously studied regular two-polariton states [37,38] and fermionized states [36]. We show that the mechanism of chaotization is very general and applicable to various many-body setups with nonparabolic dispersion of excitations. In a nutshell, the mechanism can be understood by analyzing the conservation of energy $\omega(k_1)+\omega(k_2)=2\varepsilon$ and center of mass momentum $k_1+k_2=K$ for two interacting polaritons, as shown in Figs. 1(c) and 1(d). In a conventional system with parabolic dispersion $\omega \propto k^2$, there exist just two pairs of particles with given total energy 2ε and momentum K. These two pairs can be found from the intersection of the isoenergy curve $k_1^2+k_2^2=\text{const}$ [circle in Fig. 1(c)] with the isomomentum line $k_1+k_2=$ const [blue line in Fig. 1(c)]. However, the dispersion of polaritons is strongly nonparabolic, resulting from the avoided crossing of light dispersion $\omega(k)=ck$ with the atomic resonance at $\omega=\omega_0$ [see Fig. 1(b)] [37,39,40]. Specifically, for the intermediate part of the lower polariton branch away from the Brillouin zone edge, one has $\omega(k) \propto -1/k^2$ [37], and the isoenergy curve $\omega(k_1)+\omega(k_2)=$ const acquires a more complicated hyperbolic shape [Fig. 1(d)] instead of the circle in Fig. 1(c). There exist four pairs of polaritons with a given total energy and momentum [blue line in Fig. 1(d)] instead of two pairs in Fig. 1(c). For nonparabolic dispersion, isoenergy equations $\omega(k_1)+\omega(k_2)=\text{const}$ can have complex-conjugate solutions for $k_{1,2}$ even with real total momentum and energy [see red line and green point in Fig. 1(d) that lies outside the real part of the isoenergy contour]. We prove below that the combination of polariton-polariton interactions with polariton reflections from the array edges, when $k_{1,2}\to -k_{1,2}$, makes the number of single-particle states with the same total energy and momentum arbitrarily large. We have found a chaotic nonlinear map that governs the distribution of wave vector k and thus drives chaotic two-polariton states.

Regular and irregular two-photon states.—We consider N periodically spaced qubits in a one-dimensional waveguide, characterized in the Markovian approximation by the Hamiltonian $H=\sum_{m,n=1}^{N} H_{m,n} b_m^\dagger b_n + (\chi/2)\sum_{n=1}^{N} b_n^\dagger b_n^\dagger b_n b_n$, where $H_{mn}\equiv -i\Gamma_0 e^{i\varphi|m-n|}$, $m,n=1\ldots N$. Here, b_m are the annihilation operators for the bosonic excitations of the qubits, φ is the phase acquired by light between neighboring qubits, and the parameter Γ_0 is the radiative decay rate of a single qubit. The Hamiltonian is non-Hermitian due to the radiative losses, and the coupling strength does not decay with distance. We consider subwavelength regime when $\varphi\sim 1/N\ll 1$. In the limit of large anharmonicity, when $\chi/\Gamma_0\to\infty$, the Schrödinger equation for the double-excited states $\sum_{m,n}\psi_{mn} b_n^\dagger b_m^\dagger|0\rangle$ reads as follows (see also Refs. [37,41,42] and the Supplemental Material [43])

$$H_{nn'}\psi_{n'm}+\psi_{nn'}H_{n'm}-2\delta_{nm}H_{nn'}\psi_{n'n}=2\varepsilon\psi_{nm}, \qquad (1)$$

with $\psi_{nm}=\psi_{mn}$, and $n,m=1\ldots N$. Here, the first two terms describe the propagation of the first and second polaritons, respectively. The third term accounts for their repulsion, enforcing $\psi_{nn}=0$.

Figure 2 presents three characteristic eigenstates, with the energies increasing from left to right, calculated numerically for an array with $N=120$ qubits. The top row shows Fourier transforms $|\sum_{nm}\psi_{nm}e^{-ik_x n-ik_x m}|^2$ and the bottom row presents the real-space probability densities $|\psi_{nm}|^2$. The state in Figs. 2(a) and 2(d) can be understood from the analytical model where each one of the two polaritons induces an effective periodic potential for the other one [38]. It has a regular structure with sharp localized features in real space [Fig. 2(d)] and a relatively broad distribution in the Fourier space with many discrete peaks concentrated along the isoenergy contour of a noninteracting polariton pair [37],

$$\frac{\Gamma_0\sin\varphi}{\cos k_1-\cos\varphi}+\frac{\Gamma_0\sin\varphi}{\cos k_2-\cos\varphi}=2\varepsilon, \qquad (2)$$

shown by the cyan curves in Figs. 2(a)–2(c). As such, the state in Figs. 2(a) and 2(d) consists of many single-particle states and clearly cannot be described by a simple Bethe ansatz, although it has a regular real-space wave function. The state in Figs. 2(b) and 2(e) is very different, and we will term it as a chaotic state. While it is hard to give a mathematically precise definition of chaotic states in a finite discrete system, we stress that the state shown in Fig. 2(b) has a highly irregular wave function in real space, and, at the same time its Fourier spectrum shown in Fig. 2(e) is broad and relatively homogeneous along the isoenergy contour. This is in accordance with the Berry hypothesis for chaotic states [48]. Finally, in Figs. 2(c) and 2(f) we show the fermionized two-polariton state [36]. The state is regular in real space, has eight distinct peaks in the Fourier space, and is well described by the Bethe ansatz $\psi_{nm}=\psi_{mn}\propto\cos k_1(n-\frac{1}{2})\cos k_2(m-\frac{1}{2})-(n\leftrightarrow m)$ for $n>m$. The coexistence of the fermionized regular eigenstates [Figs. 2(c) and 2(f)] with regular eigenstates [Figs. 2(a) and 2(d)] and chaotic eigenstates [Figs. 2(b) and 2(e)] for the same Hamiltonian and the same parameters is rather surprising. Our central goal is to explain this result and to identify the origin of the apparent chaotic character of the wave function in Figs. 2(b) and 2(e).

Bethe ansatz and its breakdown.—It is inconvenient to start directly from the Schrödinger equation [Eq. (1)] since the corresponding Hamiltonian matrix is dense due to long-range couplings. Instead, we use the fact that the inverse

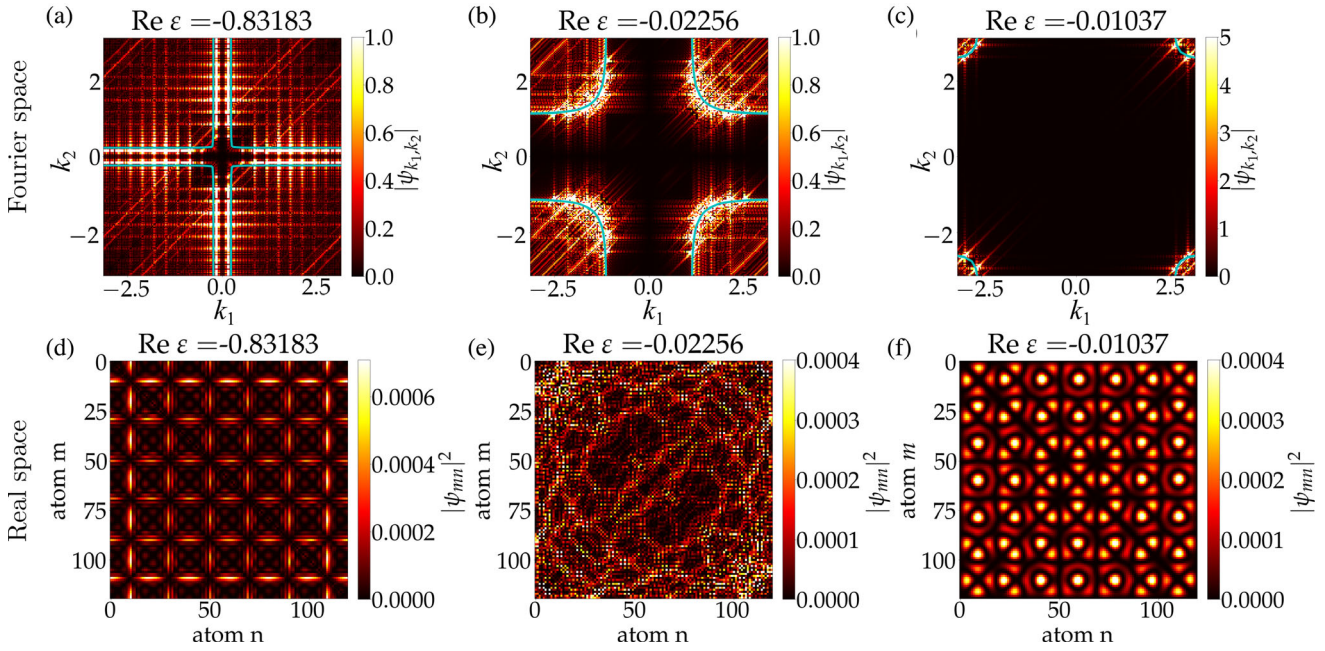

FIG. 2. (a),(b),(c) Fourier transforms and (d),(e),(f) real-space wave functions of several characteristic two-polariton states. (a),(d) Regular nonintegrable state; (b),(e) irregular chaoticlike state; (c),(f) fermionized state. The calculation has been performed for $N = 120$ qubits and $\varphi = 0.02$. Cyan curves in (a)–(c) show the isoenergy contours [Eq. (2)]. Energy is measured in units of Γ_0.

matrix H^{-1} is tridiagonal and change the basis as $\psi = H^{-1}\Psi H^{-1}$ [49] to obtain an equivalent sparse equation [37]

$$(H^{-1}\Psi + \Psi H^{-1})_{nm} - 2\delta_{nm}(\Psi H^{-1})_{nn} = 2\varepsilon(H^{-1}\Psi H^{-1})_{nm}. \tag{3}$$

We now try to solve it using a Bethe ansatz:

$$\Psi_{mn} = \sum_{K,q} A_{K,q} e^{iK(m+n)+iq|m-n|/2}, \tag{4}$$

where $A_{K,q}$ are the coefficients and the summation goes over particular values of the center of mass motion wave vector $K = (k_1 + k_2)/2$ and the relative motion wave vector $q = k_1 - k_2$ that are determined below. Each term of the ansatz Eq. (4) shall satisfy Eq. (3) at all m, n except for the diagonal region $|m - n| = 0$, 1 and the array boundaries $m,n = 1,N$. That is fulfilled if $k_{1,2} = K \pm q/2$ lies on the isoenergy contour [Eq. (2)].

First, we consider an infinite array, where the center of mass wave vector K is a good quantum number. Substituting $k_{1,2} = K \pm q/2$ in the dispersion equation [Eq. (2)], we find four inequivalent values of the relative motion wave vector $q(K)$ for any value of K. The values of q can be both real and complex (explicit expressions are given in the Supplemental Material). Real-valued solutions can be found from the intersection of the line $k_1 + k_2 = K$, describing all states with given total momentum, with the isoenergy contour [Eq. (2)] [see Fig. 1(d)]. These four solutions can be combined in Eq. (4) to satisfy Eq. (3) as shown in the Supplemental Material, which finishes the construction of the Bethe ansatz in the infinite system. However, this procedure breaks down for a finite array.

In a finite array, photons can reflect from the boundaries. To accommodate the boundaries, one should include in the Bethe ansatz the reflected waves with the wave vectors $\tilde{k}_{1,2} = -k_{1,2}$. After the reflection of one of the two photons, the new center of mass wave vector is $\tilde{K} = (\tilde{k}_1 + \tilde{k}_2)/2 = \pm(k_1 - k_2)/2 = \pm q/2$. Thus, we obtain a nonlinear map,

$$K \to \tilde{K} = \pm\frac{1}{2}q(K), \tag{5}$$

that generates new pairs of wave vectors K and $q(K)$ that must be included in the Bethe ansatz [Eq. (4)]. All the generated plane waves should be combined to satisfy the Schrödinger equation at the boundaries [50,51]. The inability to do so would indicate that the system is nonintegrable. However, the considered two-polariton problem offers one more scenario of the Bethe ansatz breakdown. Namely, the map [Eq. (5)] can generate an arbitrarily large number of wave vectors, rendering the whole Bethe ansatz construction impractical.

In the three columns of Fig. 3, we explore the map for different ranges of wave vectors $k_{1,2}$ that feature regular, chaotic, and fermionic two-polariton states. We start with Fig. 3(a), which corresponds to the situation of Fig. 2(a), where $k_1 \ll \pi$; $k_2 \gg k_1$ and the isoenergy contour is almost flat. The subsequent reflections (red lines) and the map

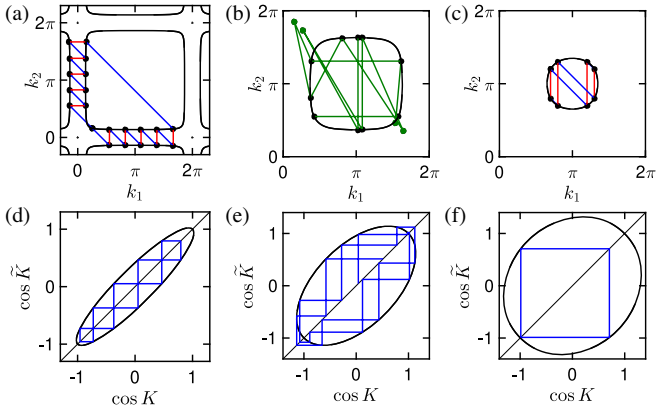

FIG. 3. Examples of subsequent application of the map [Eq. (5)] for different initial wave vectors: (a) regular 21-cycle, starting with $k_1 = 0.8, k_2 = 0.5$; (b) ergodic infinite cycle starting with $k_1 = 1.33$, $k_2 = 1.73$; (c) 8-cycle in fermionic regime starting with $k_1 = 2.2$, $k_2 = 3.8$. Red lines correspond to the reflection of one of the polaritons from the boundary; blue lines describe the wave vector exchange due to polariton-polariton interaction. Green points in (b) show real parts of complex wave vectors. For (b),(c), the vectors $k_{1,2}$ are reduced to the Brillouin zone $0 \le k_{1,2} \le 2\pi$ before the vector $K = (k_1 + k_2)/2$ is calculated. Black lines show the isofrequency contours [Eq. (2)]. The bottom panels (d)–(f) show the same cycles as in (a)–(c) for the equivalent map [Eq. (6)], tracing the evolution of the center-of-mass wave vector K.

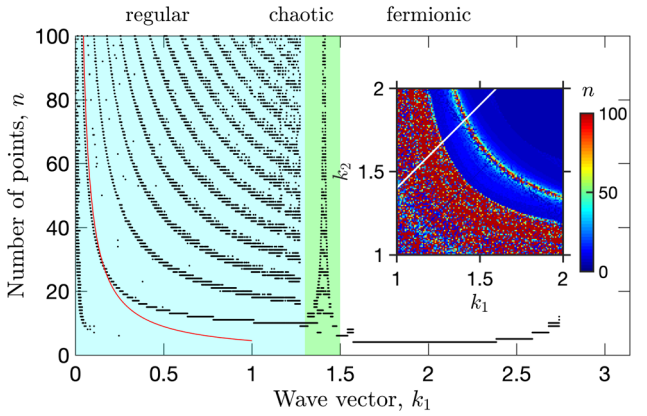

FIG. 4. Number of points n generated by the map [Eq. (5)] depending on the starting wave vector k_1 for $k_2 = k_1 + 0.4$. We used 100 iterations for each of the 1.6×10^5 starting values of $k_1 = 0.4 \ldots \pi - 0.4$ (white line in the inset). Only the points below the threshold $|\mathrm{Im}q| < 1$ have been included in the map. Red curve shows the analytical dependence $n = \sqrt{2}\pi/k_1$. Inset shows the dependence of n on both starting wave vectors k_1 and k_2 varying near the center of the Brillouin zone. The grid step is 8×10^{-3}, and 70 iterations were made for the inset.

$q(K)$ evaluation (intersection of the isoenergy contour with the blue lines $k_1 + k_2 = \text{const}$) yield two "chainsaws" of almost equidistant points. Figure 3(a) shows a specific cycle with just 21 points, but the length of cycle can be arbitrarily large, even though the corresponding real-space wave functions look regular. The set of wave vectors obtained in Fig. 3(a) explains the Fourier transform of the wave function in Fig. 2(a). It is instructive to rewrite the map [Eq. (5)] as a quadratic form depending on $\cos K$ and $\cos\tilde{K}$. For $\varphi \ll 1$, the map can be presented as

$$(\cos K - \cos\tilde{K})^2 - \frac{\varphi\Gamma_0}{\varepsilon}(\cos K \cos\tilde{K} - 1) = 0. \quad (6)$$

Figure 3(d) shows the same iterations as Fig. 3(a) for the $K \to \tilde{K}$ map [Eq. (6)].

Another scenario is realized when k_1 and k_2 are both close to the Brillouin zone edge π. The polariton dispersion is then almost parabolic [36], and the isoenergy contours [Eq. (2)] reduce to slightly deformed circles centered at $k_{1,2} = \pm\pi$ [see Figs. 3(c) and 3(f)]. As such, the map [Eq. (5)] generates just eight inequivalent points, similar to the traditional Bethe ansatz [52]. This explains the fermionic states [36] shown in Fig. 2(c). However, this consideration fails for intermediate values of wave vectors since it takes into account only two real values of q for each center of mass wave vector and ignores two other (complex) values. When the evanescent waves with complex q, K are taken into account, the maps [Eqs. (5), (6)] can generate infinite ergodic trajectories. In order to build an ergodic trajectory, we use the fact that the map [Eq. (6)] provides two values of $\cos\tilde{K}$ for each value of $\cos K$. By choosing between these two values, we can build an infinite trajectory that turns around the points $\cos K = \cos\tilde{K} = \pm 1$ and never repeats itself, as shown in Fig. 3(e). By construction, this trajectory includes evanescent waves, where $|\cos K| > 1$ and the polariton wave vectors $k_{1,2} = K \pm q/2$ are complex. This is also seen in Fig. 3(b), where green points represent complex $k_{1,2}$ that do not lie on the real isoenergy contour. Such trajectories lead to a dense irregular distribution of wave vectors in the Fourier space and explain the formation of chaotic states [Figs. 2(b) and 2(e)].

In order to examine the transition from regular to chaotic states in more detail, we plot in Fig. 4 the number of points generated by the map [Eq. (5)] depending on the initial polariton wave vector k_1 for $k_2 = k_1 + 0.4$. Three distinct ranges of wave vectors can be identified. In the range $0 \le k_1 \lesssim 1.3$, the map generates cycles of type shown in Figs. 3(a) and 3(d). The points in Fig. 4 group into "lines" that correspond to cycles with different numbers of loops made around the ellipse in Fig. 3(d). For example, the red curve $n = \sqrt{2}\pi/k_1$ shows the approximate number of points for a one-loop cycle. In our calculation, we neglected strongly evanescent waves with $|\mathrm{Im}q| > \mathrm{Im}q^* = 1$, assuming that their contribution to the wave function is exponentially weak. Such a cutoff leads to a steep decrease in the number of generated points for $k_1 \gtrsim 1.5$ (the results are not qualitatively sensitive to the cutoff value). Only a small number of wave vectors are generated, which corresponds

to the fermionized states of the type shown in Figs. 3(c) and 3(f). Finally, there is a narrow peak in the transition region, centered at around $k_1 \approx 1.4$, corresponding to the chaotic states of the type shown in Figs. 3(b) and 3(e). The inset of Fig. 4 shows the same number of generated points, depending on the values of both initial wave vectors k_1 and k_2. The calculation also reveals two distinct regions of fermionic and regular states, with a narrow chaotic region in between.

To summarize, we have obtained a nonlinear map describing polariton-polariton interactions. The number of nonevanescent waves generated by this map is a good predictor of whether a given quantum state is regular nonintegrable, chaotic, or integrable fermionized. Our findings apply to various two-particle systems and will hopefully also be useful for many-body setups. The tomography of chaotic states would require exciting and probing each qubit individually rather than through the waveguide mode [6,53], which seems feasible for modern superconducting processors with $N \gtrsim 10$ qubits [54].

The work of A. V. P. and A. N. P. (calculation and analytical description of the chaotic states) was funded by the Russian Science Foundation Project No. 20-12-00194. A. V. P. also acknowledges the support from the Russian President Grant No. MK-4191.2021.1.2.

*Corresponding author.
poddubny@coherent.ioffe.ru

[1] D. Roy, C. M. Wilson, and O. Firstenberg, Colloquium: Strongly interacting photons in one-dimensional continuum, Rev. Mod. Phys. **89**, 021001 (2017).
[2] D. E. Chang, J. S. Douglas, A. González-Tudela, C.-L. Hung, and H. J. Kimble, Colloquium: Quantum matter built from nanoscopic lattices of atoms and photons, Rev. Mod. Phys. **90**, 031002 (2018).
[3] A. F. van Loo, A. Fedorov, K. Lalumiere, B. C. Sanders, A. Blais, and A. Wallraff, Photon-mediated interactions between distant artificial atoms, Science **342**, 1494 (2013).
[4] N. V. Corzo, J. Raskop, A. Chandra, A. S. Sheremet, B. Gouraud, and J. Laurat, Waveguide-coupled single collective excitation of atomic arrays, Nature (London) **566**, 359 (2019).
[5] M. Mirhosseini, E. Kim, X. Zhang, A. Sipahigil, P. B. Dieterle, A. J. Keller, A. Asenjo-Garcia, D. E. Chang, and O. Painter, Cavity quantum electrodynamics with atom-like mirrors, Nature (London) **569**, 692 (2019).
[6] J. D. Brehm, A. N. Poddubny, A. Stehli, T. Wolz, H. Rotzinger, and A. V. Ustinov, Waveguide bandgap engineering with an array of superconducting qubits, npj Quantum Mater. **6**, 10 (2021).
[7] A. S. Prasad, J. Hinney, S. Mahmoodian, K. Hammerer, S. Rind, P. Schneeweiss, A. S. Sørensen, J. Volz, and A. Rauschenbeutel, Correlating photons using the collective nonlinear response of atoms weakly coupled to an optical mode, Nat. Photonics **14**, 719 (2020).
[8] P. M. Leung and B. C. Sanders, Coherent Control of Microwave Pulse Storage in Superconducting Circuits, Phys. Rev. Lett. **109**, 253603 (2012).
[9] H. Zheng, D. J Gauthier, and H. U. Baranger, Waveguide-QED-Based Photonic Quantum Computation, Phys. Rev. Lett. **111**, 090502 (2013).
[10] H. Zheng and H. U. Baranger, Persistent Quantum Beats and Long-Distance Entanglement from Waveguide-Mediated Interactions, Phys. Rev. Lett. **110**, 113601 (2013).
[11] A. Johnson, M. Blaha, A. E. Ulanov, A. Rauschenbeutel, P. Schneeweiss, and J. Volz, Observation of Collective SuperStrong Coupling of Cold Atoms to a 30-m Long Optical Resonator, Phys. Rev. Lett. **123**, 243602 (2019).
[12] H. J. Kimble, The quantum internet, Nature (London) **453**, 1023 (2008).
[13] M. Laakso and M. Pletyukhov, Scattering of Two Photons from Two Distant Qubits: Exact Solution, Phys. Rev. Lett. **113**, 183601 (2014).
[14] C. Noh and D. G. Angelakis, Quantum simulations and many-body physics with light, Rep. Prog. Phys. **80**, 016401 (2017).
[15] K. G. L. Pedersen and M. Pletyukhov, Few-photon scattering on Bose-Hubbard lattices, Phys. Rev. A **96**, 023815 (2017).
[16] T. Shi, Y.-H. Wu, A. González-Tudela, and J. I. Cirac, Effective many-body Hamiltonians of qubit-photon bound states, New J. Phys. **20**, 105005 (2018).
[17] K. Xu, J.-J. Chen, Y. Zeng, Y.-R. Zhang, C. Song, W. Liu, Q. Guo, P. Zhang, D. Xu, H. Deng, K. Huang, H. Wang, X. Zhu, D. Zheng, and H. Fan, Emulating Many-Body Localization with a Superconducting Quantum Processor, Phys. Rev. Lett. **120**, 050507 (2018).
[18] Z. Wang, T. Jaako, P. Kirton, and P. Rabl, Supercorrelated Radiance in Nonlinear Photonic Waveguides, Phys. Rev. Lett. **124**, 213601 (2020).
[19] I. Iorsh, A. Poshakinskiy, and A. Poddubny, Waveguide Quantum Optomechanics: Parity-Time Phase Transitions in Ultrastrong Coupling Regime, Phys. Rev. Lett. **125**, 183601 (2020).
[20] L. D. Faddeev, The new life of complete integrability, Phys. Usp. **56**, 465 (2013).
[21] J. E. Moore, A perspective on quantum integrability in many-body-localized and Yang–Baxter systems, Phil. Trans. R. Soc. A **375**, 20160429 (2017).
[22] V. E. Bunakov, Quantum signatures of chaos or quantum chaos? Phys. At. Nucl. **79**, 995 (2016).
[23] D. Ullmo, Many-body physics and quantum chaos, Rep. Prog. Phys. **71**, 026001 (2008).
[24] L. D'Alessio, Y. Kafri, A. Polkovnikov, and M. Rigol, From quantum chaos and eigenstate thermalization to statistical mechanics and thermodynamics, Adv. Phys. **65**, 239 (2016).
[25] M. Aßmann, J. Thewes, D. Fröhlich, and M. Bayer, Quantum chaos and breaking of all anti-unitary symmetries in Rydberg excitons, Nat. Mater. **15**, 741 (2016).
[26] J. Maldacena, S. H. Shenker, and D. Stanford, A bound on chaos, J. High Energy Phys. 08 (2016) 106.
[27] T. Morita, Thermal Emission from Semiclassical Dynamical Systems, Phys. Rev. Lett. **122**, 101603 (2019).

[28] K. M. Birnbaum, A. Boca, R. Miller, A. D. Boozer, T. E. Northup, and H. J. Kimble, Photon blockade in an optical cavity with one trapped atom, Nature (London) **436**, 87 (2005).
[29] E. H. Lieb and W. Liniger, Exact analysis of an interacting Bose gas. I. The general solution and the ground state, Phys. Rev. **130**, 1605 (1963).
[30] J. B. McGuire, Study of exactly soluble one-dimensional n-body problems, J. Math. Phys. (N.Y.) **5**, 622 (1964).
[31] M. Gaudin, Boundary energy of a Bose gas in one dimension, Phys. Rev. A **4**, 386 (1971).
[32] M. W. Beims, C. Manchein, and J. M. Rost, Origin of chaos in soft interactions and signatures of nonergodicity, Phys. Rev. E **76**, 056203 (2007).
[33] D. L. Shepelyansky, Chaotic delocalization of two interacting particles in the classical Harper model, Eur. Phys. J. B **89**, 157 (2016).
[34] M. Van Vessen, M. C. Santos, B. K. Cheng, and M. G. E. da Luz, Origin of quantum chaos for two particles interacting by short-range potentials, Phys. Rev. E **64**, 026201 (2001).
[35] G. Casati and T. Prosen, Mixing Property of Triangular Billiards, Phys. Rev. Lett. **83**, 4729 (1999).
[36] Y.-X. Zhang and K. Mølmer, Theory of Subradiant States of a One-Dimensional Two-Level Atom Chain, Phys. Rev. Lett. **122**, 203605 (2019).
[37] J. Zhong, N. A. Olekhno, Y. Ke, A. V. Poshakinskiy, C. Lee, Y. S. Kivshar, and A. N. Poddubny, Photon-Mediated Localization in Two-Level Qubit Arrays, Phys. Rev. Lett. **124**, 093604 (2020).
[38] A. V. Poshakinskiy, J. Zhong, Y. Ke, N. A. Olekhno, C. Lee, Y. S. Kivshar, and A. N. Poddubny, Quantum Hall phases emerging from atom–photon interactions, npj Quantum Inf. **7**, 34 (2021).
[39] E. L. Ivchenko, Excitonic polaritons in periodic quantum-well structures, Sov. Phys. Solid State **33**, 1344 (1991), http://mi.mathnet.ru/rus/ftt/v33/i8/p2388.
[40] A. Albrecht, L. Henriet, A. Asenjo-Garcia, P. B. Dieterle, O. Painter, and D. E. Chang, Subradiant states of quantum bits coupled to a one-dimensional waveguide, New J. Phys. **21**, 025003 (2019).
[41] T. Caneva, M. T. Manzoni, T. Shi, J. S. Douglas, J. I. Cirac, and D. E. Chang, Quantum dynamics of propagating photons with strong interactions: A generalized input–output formalism, New J. Phys. **17**, 113001 (2015).
[42] Y. Ke, A. V. Poshakinskiy, C. Lee, Y. S. Kivshar, and A. N. Poddubny, Inelastic Scattering of Photon Pairs in Qubit Arrays with Subradiant States, Phys. Rev. Lett. **123**, 253601 (2019).
[43] See Supplemental Materials, which include Refs. [44–47], at http://link.aps.org/supplemental/10.1103/PhysRevLett.126.203602 for the derivation details and auxiliary calculation results.
[44] Y.-X. Zhang, C. Yu, and K. Mølmer, Subradiant bound dimer excited states of emitter chains coupled to a one dimensional waveguide, Phys. Rev. Research **2**, 013173 (2020).
[45] A. V. Poshakinskiy and A. N. Poddubny, Biexciton-mediated superradiant photon blockade, Phys. Rev. A **93**, 033856 (2016).
[46] A. A. Abrikosov, Electron scattering on magnetic impurities in metals and anomalous resistivity effects, Phys. Phys. Fiz. **2**, 5 (1965).
[47] E. L. Ivchenko, *Optical Spectroscopy of Semiconductor Nanostructures* (Alpha Science International, Harrow, 2005).
[48] M. V. Berry, Regular and irregular semiclassical wavefunctions, J. Phys. A **10**, 2083 (1977).
[49] A. N. Poddubny, Quasiflat band enabling subradiant two-photon bound states, Phys. Rev. A **101**, 043845 (2020).
[50] M. T. Batchelor, The Bethe ansatz after 75 years, Phys. Today **60**, No. 1, 36 (2007).
[51] J. M. Zhang, D. Braak, and M. Kollar, Bound States in the Continuum Realized in the One-Dimensional Two-Particle Hubbard Model with an Impurity, Phys. Rev. Lett. **109**, 116405 (2012).
[52] S. Longhi and G. Della Valle, Tamm–Hubbard surface states in the continuum, J. Phys. Condens. Matter **25**, 235601 (2013).
[53] E. Kim, X. Zhang, V. S. Ferreira, J. Banker, J. K. Iverson, A. Sipahigil, M. Bello, A. González-Tudela, M. Mirhosseini, and O. Painter, Quantum Electrodynamics in a Topological Waveguide, Phys. Rev. X **11**, 011015 (2021).
[54] Y. Ye *et al.*, Propagation and Localization of Collective Excitations on a 24-Qubit Superconducting Processor, Phys. Rev. Lett. **123**, 050502 (2019).